Biophysical and functional characterization of Norrin signaling through Frizzled4

Injin Bang[a,1], Hee Ryung Kim[b,1], Andrew H. Beaven[c,2], Jinuk Kim[a], Seung-Bum Ko[a], Gyu Rie Lee[d,3], Wei Kan[e], Hasup Lee[d,4], Wonpil Im[f,g], Chaok Seok[d], Ka Young Chung[b,5], and Hee-Jung Choi[a,5]

[a]Department of Biological Sciences, Seoul National University, 08826 Seoul, Republic of Korea; [b]School of Pharmacy, Sungkyunkwan University, 16419 Suwon, Republic of Korea; [c]Department of Chemistry, The University of Kansas, Lawrence, KS 66047; [d]Department of Chemistry, Seoul National University, 08826 Seoul, Republic of Korea; [e]Department of Structural Biology, Stanford University School of Medicine, Stanford, CA 94305; [f]Department of Biological Sciences, Lehigh University, Bethlehem, PA 18015; and [g]Department of Bioengineering, Lehigh University, Bethlehem, PA 18015

Edited by Jeremy Nathans, Johns Hopkins University, Baltimore, MD, and approved July 17, 2018 (received for review April 5, 2018)

Wnt signaling is initiated by Wnt ligand binding to the extracellular ligand binding domain, called the cysteine-rich domain (CRD), of a Frizzled (Fzd) receptor. Norrin, an atypical Fzd ligand, specifically interacts with Fzd4 to activate β-catenin–dependent canonical Wnt signaling. Much of the molecular basis that confers Norrin selectivity in binding to Fzd4 was revealed through the structural study of the $Fzd4_{CRD}$–Norrin complex. However, how the ligand interaction, seemingly localized at the CRD, is transmitted across full-length Fzd4 to the cytoplasm remains largely unknown. Here, we show that a flexible linker domain, which connects the CRD to the transmembrane domain, plays an important role in Norrin signaling. The linker domain directly contributes to the high-affinity interaction between Fzd4 and Norrin as shown by ∼10-fold higher binding affinity of $Fzd4_{CRD}$ to Norrin in the presence of the linker. Swapping the Fzd4 linker with the Fzd5 linker resulted in the loss of Norrin signaling, suggesting the importance of the linker in ligand-specific cellular response. In addition, structural dynamics of Fzd4 associated with Norrin binding investigated by hydrogen/deuterium exchange MS revealed Norrin-induced conformational changes on the linker domain and the intracellular loop 3 (ICL3) region of Fzd4. Cell-based functional assays showed that linker deletion, L430A and L433A mutations at ICL3, and C-terminal tail truncation displayed reduced β-catenin–dependent signaling activity, indicating the functional significance of these sites. Together, our results provide functional and biochemical dissection of Fzd4 in Norrin signaling.

Frizzled 4 | linker domain | Norrin | Dishevelled | signaling

Wnt signaling plays an important role in embryonic development, tissue homeostasis, and cell proliferation in adult tissues. Aberrant Wnt signaling causes various human diseases such as cancer and neurodegenerative disease (1). Frizzled (Fzd) receptors on the cell surface recognize Wnt ligands by their extracellular cysteine-rich domain (CRD) (2) and transmit their signal to the cytoplasm. Although Wnt is the main ligand for the Fzd family, Fzd4 has an atypical and highly specific ligand called Norrin. Norrin functions as a growth factor that is especially required for angiogenesis in the eye (3), and mutations in the gene encoding human Norrin are associated with Norrie disease, which impairs vision (4). Specific Norrin binding to Fzd4 (5) activates the β-catenin–dependent canonical Wnt signaling pathway, in which Dishevelled (Dvl), as a cytoplasmic downstream molecule, is shown to interact with intracellular loop 3 (ICL3) and the highly conserved KTXXXW motif of Fzd (6, 7).

From a structural point of view, Norrin is completely different from Wnt. Norrin has a cystine-knot motif and forms a homodimer through intermolecular disulfide bonds (8, 9). Unlike Wnt, in which a palmitoleic acid lipid group is attached at a conserved serine (10), Norrin is not lipid-modified. The molecular basis of the specific interaction of Norrin with Fzd4 was shown by the crystal structures of the $Fzd4_{CRD}$–Norrin complex, in which two CRD molecules interact with a head-to-tail Norrin dimer in a 2:2 stoichiometry (9). A structural comparison of the $Fzd4_{CRD}$–Norrin complex with the $Fzd8_{CRD}$–*Xenopus* Wnt8 (XWnt8) complex showed that the binding surface on the CRD for Norrin overlaps with that for the Wnt finger loop, but the lipid-mediated interaction of XWnt8 is missing in Norrin (9, 10).

Most structural studies on the Fzd family have focused on the extracellular domain to understand how Fzd achieves its ligand specificity. To our knowledge, no structural information about the Fzd transmembrane domain (TMD) or the linker domain between the CRD and the TMD is available yet. The linker domain is highly divergent among Fzd subtypes, varying in length from approximately 40 aa in Fzd4 to 100 aa in Fzd8, and in sequence as well. The functional role of the linker domain has not yet been studied to our awareness.

Although X-ray crystallography remains the favorite tool for structural evaluation of membrane proteins, it is, in general, a challenging and time-consuming approach, and the crystal structure provides only a thermodynamically static view of the protein. The structural dynamics of a protein are as important as its static structure in understanding its function. Hydrogen/deuterium exchange MS (HDX-MS) has been successfully used to probe the

Significance

Wnt signaling has a broad spectrum of effects on cellular physiology and diseases like cancer. Much of the specificity and regulation mechanism of the Frizzled (Fzd) family, the main receptor of the Wnt pathway, remains elusive, but exploiting the activation mechanism of Fzd is pivotal to understanding the Wnt signaling pathway. Here, by using biophysical and biochemical techniques, we identify the key conformational changes that occur as the Norrin ligand binds to Fzd4, and we show the functional implications of the involved regions. We also reveal that the linker region plays an important role in communicating ligand binding with cytoplasmic signaling. Our observations offer insight into the activation mechanism of the Fzd family and the regulation of the Wnt signaling pathway.

Author contributions: H.-J.C. designed research; I.B., H.R.K., J.K., and S.-B.K. performed research; W.K. and K.Y.C. contributed new reagents/analytic tools; I.B., H.R.K., A.H.B., G.R. L., W.K., H.L., W.I., C.S., and K.Y.C. analyzed data; and I.B. and H.-J.C. wrote the paper.

The authors declare no conflict of interest.

This article is a PNAS Direct Submission.

[1]I.B. and H.R.K. contributed equally to this work.

[2]Present address: Department of Biomedical Engineering, University of Minnesota, Minneapolis, MN 55455.

[3]Present address: Department of Biochemistry, University of Washington, Seattle, WA 98195.

[4]Present address: Organic Material Lab, Samsung Advanced Institute of Technology, Gyeonggi-do, 443-803 Suwon, Republic of Korea.

[5]To whom correspondence may be addressed. Email: kychung2@skku.edu or choihj@snu.ac.kr.

This article contains supporting information online at www.pnas.org/lookup/suppl/doi:10.1073/pnas.1805901115/-/DCSupplemental.

Published online August 13, 2018.

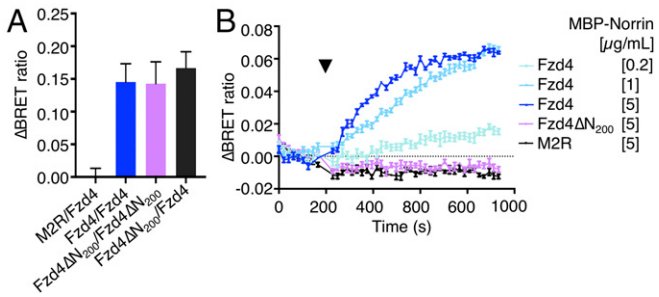

Fig. 1. Fzd4 oligomerization in vivo observed with BRET. All measurements were done with at least four repeats, and the error bars are drawn with SEM. (*A*) Each ΔBRET ratio was calculated by taking the BRET ratio of a structurally unrelated muscarinic receptor 2 (M2R) and Fzd4 pair as the background ratio. Transfected receptor pair is labeled below in RLuc8-/YFP-tagged order. (*B*) Kinetic measurement of the BRET ratio is plotted with a black arrow marking the injection time point of MBP–Norrin. For M2R and Fzd4ΔN$_{200}$, only the data at the highest MBP–Norrin concentration (5 μg/mL) are plotted because similar results were obtained at all three concentrations.

ligand-mediated dynamic conformational change of G protein-coupled receptors (GPCRs) (11). In this study, we evaluated the conformational change of Fzd4 upon Norrin binding by using HDX-MS in combination with computational structure modeling. We also revealed that full-length Fzd4 binds to Norrin ∼10 times more tightly than the CRD itself, and that the linker region is responsible for this tight binding. Further functional assays were performed to assess whether the linker and ICL3 regions, which show that the ligand-induced conformational dynamics are related to biological function. Our studies provide an important allosteric activation mechanism of Fzd4 in Norrin signaling.

Results and Discussion

Oligomeric State of Fzd4. Although the crystal structures of Fzd4$_{CRD}$ itself or in complex with Norrin are available (9, 12), no structure of full-length Fzd has been reported to characterize its interaction with the ligand. As the first step to study the structural dynamics of Fzd4 upon Norrin binding, we purified full-length Fzd4 (hereafter simply Fzd4) and made a complex with Norrin (*SI Appendix*, Fig. S1). We examined the oligomeric states of purified Fzd4 and the Fzd4–Norrin complex by using a multiangle light scattering (MALS) system (*SI Appendix*, Fig. S2). The molecular weights of Fzd4 alone and the Fzd4–Norrin complex were calculated to be 51 kDa and 128 kDa, respectively, suggesting that Fzd4 forms a Norrin-induced dimer, whereas Fzd4 alone remains a monomer in vitro.

Whereas the purified Fzd4 from an insect cell culture was a monomer, we observed oligomeric Fzd4 in vivo by using a bioluminescence resonance energy transfer (BRET) assay (Fig. 1*A*), consistent with previous reports (8, 12). The discrepancy in the oligomeric states of Fzd4 in vitro and in vivo could be caused by the purification procedure being too harsh for a dimer to withstand and the presence of endogenous ligands and unsaturated fatty acid in vivo that can stimulate Fzd4 oligomerization (12, 13). To exclude the effect of endogenous ligands or fatty acyl groups on the oligomeric state of Fzd4 in vivo, a BRET assay was performed with a CRD-deleted Fzd4 (Fzd4ΔN$_{200}$) construct. As shown in Fig. 1*A*, Fzd4ΔN$_{200}$ gave a similar BRET signal to Fzd4, proving that the Fzd4 TMD by itself has the ability to form a dimer. This finding is in line with a previous report showing that Fzd6 forms a homodimer through a dimeric interface between TM4 and TM5 helices (14).

To investigate the effect of Norrin binding on Fzd4 oligomerization in vivo, BRET signals were monitored after an exogenous treatment of Norrin fused to a maltose binding protein (MBP) for stability. As MBP–Norrin was added, an increased BRET signal was observed for Fzd4 in a dose-dependent manner, whereas Fzd4ΔN$_{200}$ and muscarinic receptor 2 (M2R) did not show any response to Norrin treatment (Fig. 1*B*). This implies that further oligomerization of Fzd4 above the basal level can be enhanced by Norrin in vivo, probably through its dimeric form. Recently, the Wnt5a ligand was shown to induce Fzd4 oligomerization through its lipid moiety (12). Although Fzd4 oligomerization appears to be the common response to Norrin and Wnt, the molecular mechanism of Fzd4 oligomerization by these ligands likely differs because of their structural differences.

Structural Modeling of Fzd4–Norrin Complex. To better visualize how Fzd4 interacts with Norrin, nine candidate model structures were generated by computational modeling that used template-based modeling (TBM), domain docking, linker modeling, and molecular dynamics (MD) simulations (*SI Appendix*, Fig. S3). A dimeric TM structure of Smoothened receptor (SMO), which belongs to the class F GPCR family, along with Fzd [Protein Data Bank (PDB) ID code 4JKV] (15) and a Fzd4$_{CRD}$–Norrin complex structure (PDB ID code 5BQC) (9), were used as templates for domain structure building by TBM. The main element of variation among our model structures was the rotation angle (ρ) of CRD-Norrin relative to the TMD (*SI Appendix*, Fig. S4). MD simulations were carried out to monitor the stability of these nine conformations in the lipid environment. In all of the models, over the second half (10 ns) of the simulation time, relatively high structural fluctuations occurred in the CRD and loop regions, whereas low variation occurred in the TMD (*SI Appendix*, Fig. S5). Models 7 and 9 showed the lowest Δρ of all of the models and the lowest total rmsd from the initial model structures after MD simulations, implying the greatest stability (*SI Appendix*, Fig. S5 and Table S1). Therefore, they were chosen as representative model structures of the Fzd4–Norrin complex (Fig. 2 and *SI Appendix*, Table S2). Both

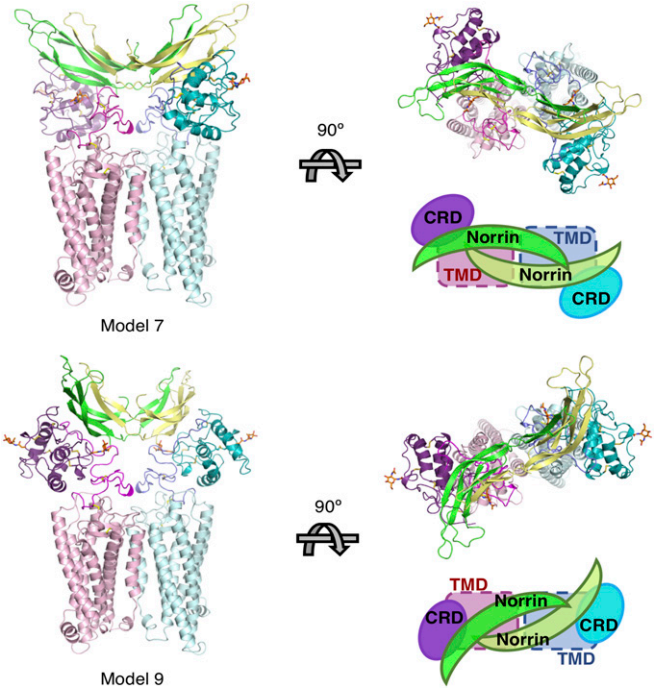

Fig. 2. Two representative computational models of Fzd4–Norrin complex. Two molecules of Norrin are shown in green and yellow-green. One Fzd4 chain is in magenta and the other is in cyan. For clarity, both CRDs are colored in darker shades. Both models were aligned against the TMDs and are shown in the same orientation. Eight disulfide bonds in each Fzd4 are shown in yellow sticks, and two molecules of GlcNAc, which were identified in the crystal structure of Fzd4$_{CRD}$ (PDB ID code 5BQC), are shown in orange sticks. Schematic drawings were made for each top view.

models contain eight intramolecular disulfide bonds: five within the CRD (C45–C106, C53–C99, C90–C128, C117–C158, C121–C145), one in the linker domain (C181–C200), one between the linker and the extracellular loop 1 (ECL1; C204–C282), and one between the ECL2 and TM3 (C302–C377). Although two N-linked glycans on the CRD were not included in our modeling, structural alignment of the crystal structures of $Fzd4_{CRD}$ with our models shows that there is no potential steric hindrance of bulky glycans with Fzd4 or Norrin in our final models (Fig. 2).

A comparison of the Fzd4 model with the SMO structure revealed one striking difference. Whereas SMO has a characteristically long TM6 that extends into extracellular space, Fzd4 seems to lack such a feature (*SI Appendix*, Fig. S6). The extended TM6 helix in SMO, together with ECL3, interacts with the CRD, holding it in a relatively fixed orientation (16, 17). Although a fully active state of the SMO structure is unavailable, a comparison of apo- and antagonist-bound structures of SMO suggests that movement of the extracellular region of TM6 by antagonist binding could contribute to the allosteric influence between the CRD and TMD (16, 17). On the contrary, Fzd4 would have a different form of allosteric modulation between the CRD and TMD because Fzd4 is predicted to have much shorter TM6 and ECL3 (*SI Appendix*, Fig. S6). Compared with SMO, Fzd subtypes have a long linker between CRD and TM1 of various sequence and length. Interestingly, our structure and energy analysis suggest that the linker region contributes to the binding of Norrin. The interactive energy of $Fzd4_{CRD}$ with the linker domain ($Fzd4_{CRDlinker}$; residues 41–203) for Norrin calculated from model 9 was 63.3 kcal·mol^{-1}, which was similar to that of Fzd4 (−69.5 kcal·mol^{-1}), whereas that of $Fzd4_{CRD}$ was much lower (−46.0 kcal·mol^{-1}). Details on the functional role of the linker domain will be discussed later.

Conformational Dynamics of Fzd4 upon Norrin Binding. To address the structural dynamics of Fzd4 upon Norrin binding, an HDX-MS experiment was performed. The HDX-MS data of ligand-free Fzd4 were consistent with the proposed serpentine structure (*SI Appendix*, Fig. S7). Ordered or buried regions, such as TM helices, had lower deuterium exchange levels than in flexible or exposed regions, including linker, ICLs, ECLs, and C-terminal tail regions.

To analyze the conformational change of Fzd4 upon Norrin binding, the HDX-MS profiles of ligand-free and Norrin-bound Fzd4 were compared. Unfortunately, we could not obtain peptidic peptides from $Fzd4_{CRD}$–Norrin interface (i.e., G57, T107–P113, and Q151–P174 based on the crystal structures of the $Fzd4_{CRD}$–Norrin complex) (9), and therefore we could not measure HDX profiles in the Norrin-binding interface. Instead, we observed HDX profiles of other regions, including the linker and ICL3. Norrin binding induced increased deuterium uptake in five regions of Fzd4 (Fig. 3*A*): the linker (residues 191–200), two sites in ECL1 (residues 285–292 and 270–278), ICL3 (residues 420–432), and the C terminus of TM6 (residues 457–464). ICL3, which is located far from the ligand binding site, showed a change in HDX profile, implying the transmission of the conformational change through the TMD upon Norrin binding at the extracellular domain.

Our HDX data clearly show that Norrin binding significantly affects the conformation of extracellular (i.e., linker, ECL1, and C terminus of TM6) and intracellular (i.e., the N terminus of TM6 and ICL3) regions. Typical GPCR activation, as characterized in mostly class A GPCRs, can be summarized by three major features: large outward movement of the cytoplasmic part of TM5 and TM6, rearrangement of TM7 around the NPXXY motif, and a broken "ionic lock" between the DRY motif in TM3 and the arginine in TM6 (18–20). Because the Fzd family lacks an NPXXY motif and a DRY motif, how the intracellular region changes as it is activated is of keen interest. Our HDX-MS data provides a clue into the structural dynamics of Fzd4 in response to Norrin.

HDX-MS Kinetic Property of Fzd4 Helix 8 and Its Functional Role in Norrin Signaling. Helix 8 of Fzd4 showed an interesting HDX-MS profile (Fig. 3*B*). Under a physiological condition, most proteins

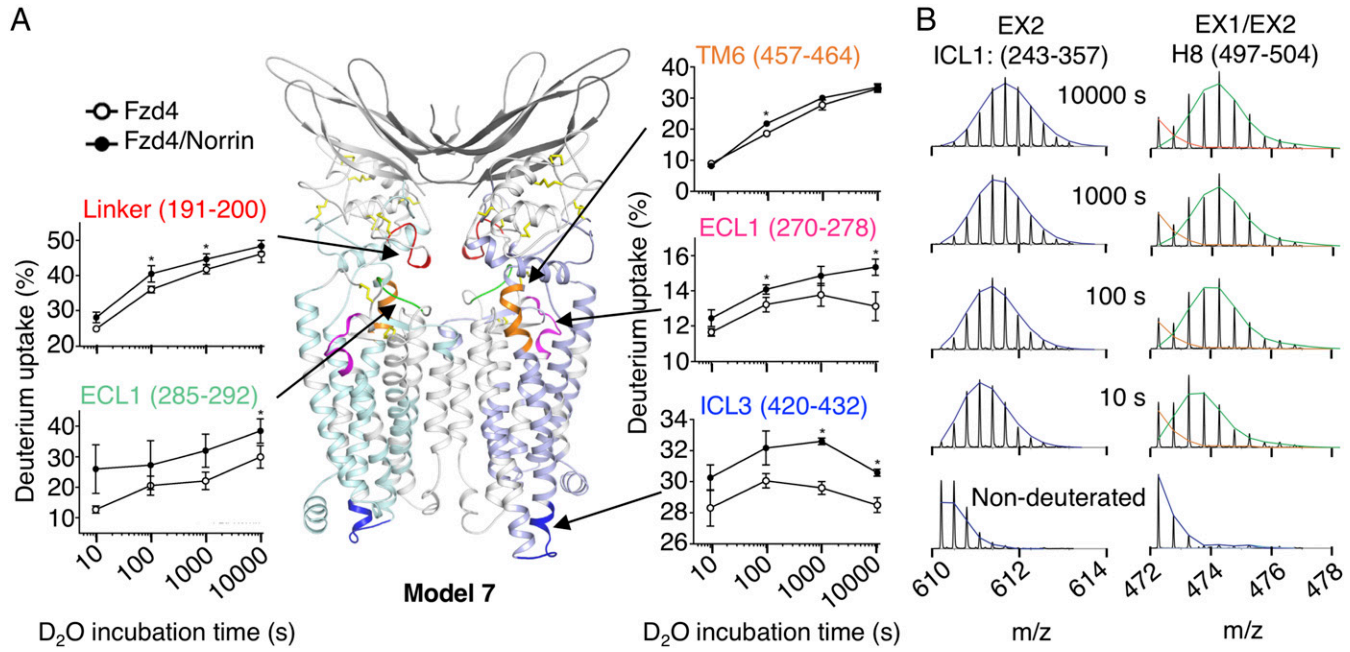

Fig. 3. HDX-MS result for Fzd4. (*A*) Differences in deuterium uptake observed for Fzd4 upon Norrin binding is noted on model 7. Whereas two Fzd4 molecules are in light green and light blue, the uncolored white patches represent the regions with no peptides identified by MS. Disulfide bonds are shown as yellow sticks. Norrin dimer is colored with light and dark gray. The peptides with altered HDX upon Norrin binding are color-coded (red, magenta, green, blue, and orange) and marked on the model. Next to the model, the deuterium uptake plots of the color-coded peptides are shown. Error bars represent SEM of three to six independent experiments. (*Significant at $P < 0.05$.) (*B*) Mass spectra of peptides from ICL1 (*Left*) and helix 8 (*Right*) showing a binomial and a bimodal isotropic distribution, respectively, are presented.

undergo fast local unfolding/refolding events (much faster than the HDX rate), which generate EX2 kinetics presented as a binomial isotropic distribution in the mass spectrum (11). On the contrary, EX1 kinetics are achieved when the unfolding/refolding rate is considerably slower than the HDX rate, and exhibits a bimodal distribution (21). Whereas all other peptides from Fzd4 showed a binomial isotropic distribution, peptide 497–504 from helix 8 showed a bimodal isotropic distribution (Fig. 3*B*), suggesting conformational heterogeneity. Because the intensity and the *m*/*z* of the faster exchanging conformer increased as deuterium exposure increased, it is evident that the region 497–504 underwent a mixture of EX1/EX2 kinetics, reflecting the partial unfolding of helix 8. In the case of β_2AR or rhodopsin, helix 8 forms a stable α-helix, and previous HDX-MS analyses did not report EX1 kinetics from helix 8 of these receptors (21). It is not clear whether partial unfolding of helix 8 is Fzd4-specific or a general characteristic of the Fzd family. One interesting clue is that peptide 497–504 contains the KTXXXW motif, which is conserved in all Fzd subtypes and known to be important for the interaction with Dvl (6, 7). Far-UV CD and an NMR study of the C-tail of Fzd1 showed that the C-tail peptide, including the KTXXXW motif, is unstructured in an aqueous environment, whereas the major population forms an α-helix in a detergent solution with micelles present, suggesting that Fzd helix 8 exhibits micelle-dependent conformational change (22). In our experiment with Fzd4, partial unfolding of helix 8 was observed in the presence of micelles.

We inspected the functional role of the KTXXXW motif by using two C-terminal truncated mutations: $Fzd4_{504}$, whose last amino acid is W504 of KTXXXW motif, and $Fzd4_{507}$, which contains three extra amino acids after the KTXXXW motif. Consistent with a previous report (23), $Fzd4_{504}$ showed a dramatically reduced Norrin signaling, whereas the activity of $Fzd4_{507}$ was similar to that of the WT (*SI Appendix*, Fig. S8). Reduced Norrin signaling of $Fzd4_{504}$ may relate to a defect in the interaction with Dvl, as demonstrated by a BRET assay (*SI Appendix*, Fig. S9). Previous studies using the peptide derived from the Fzd7 C-terminal tail showed that the KTXXXW motif interacts with the Dvl PDZ domain, and deleting the residues N- or C-terminal to the KTXXXW motif changes the secondary structure of the peptide, leading to a reduced binding affinity to Dvl (7). In our HDX experiment, we could not detect the kinetic change in the folding of helix 8 upon Norrin binding, possibly because of the absence of Dvl. Further study is required to validate the link between the kinetic dynamics of helix 8 and the interaction with Dvl.

Contribution of Fzd4 Linker Region on Norrin Binding. Based on our calculated interactive energy (discussed earlier), and given how the signal from ligand binding needs to be propagated to the cytoplasm, we reasoned that the linker might be involved in the ligand interaction to mediate the signal transmission to the TMD. To investigate if other regions than the CRD contribute to the interaction with Norrin, we compared the binding affinities of $Fzd4_{CRD}$ and Fzd4 for MBP–Norrin by using a gel filtration assay (Fig. 4*A*). When 1 μM MBP–Norrin was mixed with 1 μM $Fzd4_{CRD}$ or Fzd4 and injected into the gel filtration column, only Fzd4 eluted together with MBP–Norrin. $Fzd4_{CRD}$ coeluted with MBP–Norrin at a higher concentration, 10 μM (*SI Appendix*, Fig. S10), revealing that Fzd4 binds to Norrin more tightly than $Fzd4_{CRD}$. To test if the linker domain is involved in tighter binding, $Fzd4_{CRDlinker}$ was purified and used for the gel filtration assay. Unlike $Fzd4_{CRD}$, $Fzd4_{CRDlinker}$ was coeluted with MBP–Norrin at the 1-μM concentration (Fig. 4*A*). A series of gel filtration assays were performed to test if $Fzd4_{CRDlinker}$ and Fzd4 have a similar affinity to Norrin. Both complexes dissociated at a similar concentration (*SI Appendix*, Fig. S11), suggesting that $Fzd4_{CRDlinker}$ has full affinity to Norrin. For a quantitative analysis of binding affinity, the K_d values of $Fzd4_{CRD}$ and $Fzd4_{CRDlinker}$ for MBP–Norrin were measured by microscale thermophoresis (MST) experiments (Fig. 4*B*). Consistent with the gel filtration assays, $Fzd4_{CRDlinker}$ binds to Norrin more strongly than $Fzd4_{CRD}$, with a K_d of 260 nM, whereas the K_d of $Fzd4_{CRD}$ is 2.0 μM.

Previously, the affinity of $Fzd4_{CRD}$ for Norrin or MBP–Norrin was measured as 1.1 μM by a surface plasmon resonance (SPR) experiment and 11 nM by an AlphaScreen assay (8, 9). This discrepancy was attributed to the use of the monomeric $Fzd4_{CRD}$ in the SPR experiment, in contrast to the use of Fc-fused dimeric $Fzd4_{CRD}$ in the AlphaScreen assay. $Fzd4_{CRD}$, $Fzd4_{CRDlinker}$, and Fzd4, used in our binding assays, were purified as monomers, as confirmed by MALS analysis (*SI Appendix*, Figs. S2 and S12). Thus, we can safely conclude that the difference in the affinity to Norrin measured in our binding assays did not originate from different oligomeric states. Therefore, our results clearly show that $Fzd4_{CRDlinker}$ and Fzd4 have similar affinity for Norrin, whereas $Fzd4_{CRD}$ has an approximately 10-fold lower affinity.

Functional Roles of the Linker and ICL3 of Fzd4 in Norrin Signaling. As the importance of the linker became evident, we analyzed the sequences of the linker domain between the conserved CRD and TMD in the Fzd subtypes. Sequence alignment of the linker domain shows an interesting feature, that Fzd4 has unique linker sequences especially in the region between two Cys residues making intramolecular disulfide bond (C181–C200), whereas other Fzd subtypes have relatively conserved sequences within their

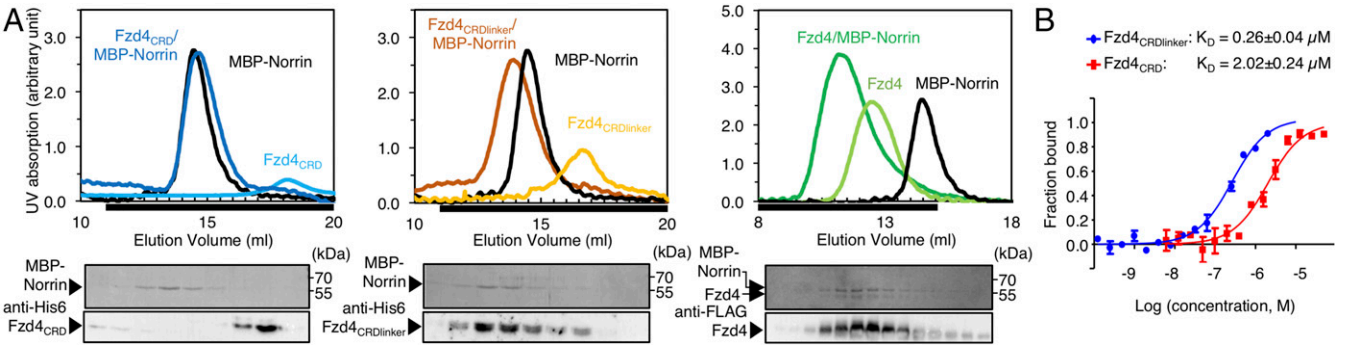

Fig. 4. In vitro binding assays between Norrin and Fzd4. (*A*) The size exclusion chromatography profile (*Top*), Coomassie-stained SDS/PAGE gel (*Middle*), and Western blot (*Bottom*) of each complex are shown. MBP–Norrin is plotted in black for all three profiles. $Fzd4_{CRD}$ is in sky blue, $Fzd4_{CRDlinker}$ in yellow, and full-length Fzd4 in green. The complexes are in a darker corresponding shade. Fractions marked by the black bar below the *x*-axis were loaded on SDS/PAGE gel. $Fzd4_{CRD}$ and $Fzd4_{CRDlinker}$ were detectable only with a Western blot. Although Fzd4 bands were visible with Coomassie staining, Fzd4 was verified with an anti-Flag antibody in a Western blot. (*B*) MST experiments were done to measure the binding affinity of $Fzd4_{CRD}$ and $Fzd4_{CRDlinker}$ for MBP–Norrin, and their binding curves are shown in red and blue, respectively. Error bars represent SD of three independent experiments.

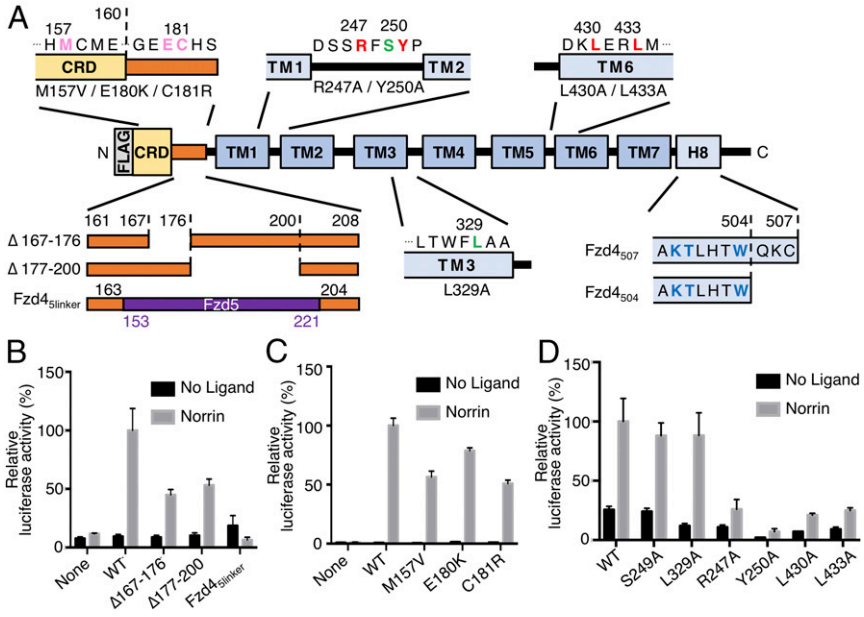

Fig. 5. Functional assessment of various Fzd4 mutations. (*A*) Schematic view of all Fzd4 constructs used for functional and binding assays. The conserved KTXXXW motif is colored blue. Based on our mutational studies, functionally significant residues at the cytoplasmic region are colored red, whereas insignificant ones are in green. FEVR-associated mutations tested in our assays are colored pink. Orange colored region represents the Fzd4 linker domain. (*B–D*) The effects of Fzd4 mutations on Norrin signaling were investigated. The bar graphs are plotted with SEM of at least four repeats. Luciferase activities of the linker deletion and the linker swap mutations are shown in *B*, and those of FEVR-associated mutations and point mutations at ICL regions are shown in *C* and *D*, respectively.

phylogenetic subgroups (*SI Appendix*, Fig. S13). To further assess whether the linker domain is functionally important in Norrin signaling, we designed two linker-deleted mutations at designated positions, Δ167–176 and Δ177–200 (Fig. 5*A* and *SI Appendix*, Fig. S14) and measured the level of canonical signaling activity of each mutation. We observed an activity decrease in both deletion mutants (Fig. 5*B*). In our calculated models, several residues in the 167–176 region (E166, V167, L169, I175) were found to make direct contacts with Norrin, whereas the hydrophobic residues V184, I192, and V201 in the other part of the linker were shown to interact with ECL1, which could contribute to Norrin binding indirectly. A previous SPR experiment that measured the binding affinity between $Fzd4_{CRD}$ and Norrin used the CRD, which was defined differently from ours, containing part of the linker (residues 43–179) (9). The K_d of 1.1 μM from that experiment is similar to our K_d for $Fzd4_{CRD}$, given that they were measured by different methods, and much higher than that for $Fzd4_{CRDlinker}$, suggesting that the full-length linker is required to achieve the full affinity for Norrin. Then, we tested the activity of the Fzd4 construct with a linker swap ($Fzd4_{5linker}$), in which the Fzd4 linker (residues 164–203) was replaced with the Fzd5 linker (residues 153–221; Fig. 5*A* and *SI Appendix*, Fig. S15). If the CRD is the only ligand binding domain and determines ligand specificity, a linker swap construct would still transmit Norrin signaling through the CRD. As shown in Fig. 5*B*, the linker swap completely eliminated the Fzd4 response to Norrin, demonstrating that the Fzd4 linker has a specific role in Norrin signal transduction. Purified $Fzd4_{CRD}$ with the Fzd5 linker ($Fzd4_{CRD5linker}$) showed lower binding affinity for Norrin than $Fzd4_{CRDlinker}$, with a K_d of 1.8 μM (*SI Appendix*, Fig. S16), suggesting that the loss of Norrin signaling of $Fzd4_{5linker}$ is related to a defect in Norrin binding. This result again proves the importance of the linker for the interaction with Norrin.

Several single missense mutations in Fzd4 have been found in patients with familial exudative vitreoretinopathy (FEVR) (5, 24), and four of them, the E180K, C181R, C204Y, and C204R mutations, are located in the linker domain. Each Cys mutant may cause a structural defect by missing a disulfide bond, leading to a defect in Norrin binding. The effect of the E180K and C181R mutations on Norrin signaling was investigated by using a TOPFlash assay with the M157V FEVR-associated mutation in the CRD as a control because it was previously shown to affect the Norrin signaling (5). Three FEVR-associated mutations, M157V, E180K, and C181R, displayed 20–50% loss of WT signaling activity (Fig. 5*C*), indicating the importance of these residues in Norrin signaling. In vitro binding assay of $Fzd4_{CRDlinker}$ with the E180K mutation showed similar but slightly lower affinity to Norrin (K_d of 290 nM), compared with WT $Fzd4_{CRDlinker}$, suggesting that E180 in the linker does not contribute to the Norrin binding directly (*SI Appendix*, Fig. S17).

Next, we assessed the ICLs of Fzd4 that are suspected to be important in Wnt signaling (7, 25). Based on our HDX-MS results in combination with a previous report about eight key residues identified to be crucial for Dvl recruitment, we designed four point mutations: R247A and Y250A at ICL1 and L430A and L433A at ICL3 (25, 26). Two more mutations, S249A and L329A, located on ICL1

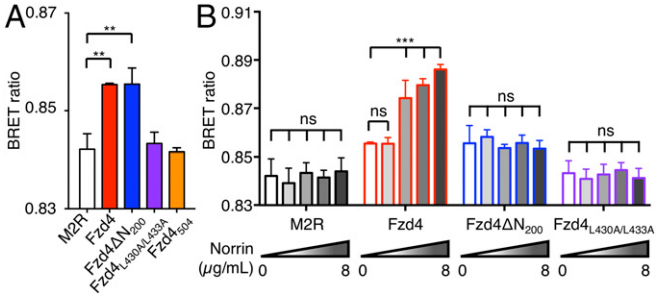

Fig. 6. BRET assays showing the interaction between YFP-Dvl2 and various Fzd4-RLuc mutations. All graphs are plotted with SEM of five repeats. (*A*) Measurements were made in the absence of Norrin to show basal level interaction. (**Significant at $P < 0.01$; ns, not significant.) (*B*) The effect of Norrin on BRET between each Fzd4 construct and Dvl2 was investigated by adding an increasing amount of Norrin (0, 0.1, 1, 5, 8 μg/mL) in each BRET assay. (***Significant at $P < 0.001$.)

and ICL2, respectively, were made as functionally silent mutations (Fig. 5*A* and *SI Appendix*, Fig. S14). Whereas S249A and L329A did not show a significant signal change in the TOPFlash assay, the other four mutations (R247A, Y250A, L430A, L433A) showed dramatically reduced activity (Fig. 5*D*), suggesting that these amino acids are important for canonical signaling by Norrin. It is notable that L430 and L433, which are located in the region showing Norrin-induced conformational change, are functionally important for Norrin signaling. In a previous study using Fzd5 ICL3 peptide, corresponding Leu residues were shown to be critical for Dvl binding (25). To investigate the Norrin-dependent interaction between Fzd4 and Dvl, BRET assays were performed by using $Fzd4_{L430A/L433A}$, $Fzd4\Delta N_{200}$, and Fzd4. In basal state, BRET ratio from $Fzd4\Delta N_{200}$ is similar to that from Fzd4 and higher than those from M2R, $Fzd4_{L430A/L433A}$, and $Fzd4_{504}$ (Fig. 6*A*). Previous reports showed that Dvl can colocalize with Fzd4 when coexpressed (7, 27), which explains the basal BRET signal, and we suspect the ICL3 mutations and C-tail truncation completely lost their ability to interact with Dvl. WT Fzd4, and not $Fzd4\Delta N_{200}$, showed a Norrin-induced BRET increase (Fig. 6*B*), implying the Norrin-dependent recruitment of Dvl2.

As shown by our functional assays using Fzd4 mutations, it is evident that L430 and L433 in ICL3 and C-tail are important for Dvl binding. We also show that the linker domain is required for the specific and high-affinity interaction with Norrin and is important for transducing the canonical signal in response to Norrin.

Conclusion

In summary, we demonstrated that the linker region of Fzd4 contributes to a high-affinity interaction with Norrin and signaling. In vitro binding assays showed that the $Fzd4_{CRDlinker}$ binds to Norrin approximately 10 times more strongly than $Fzd4_{CRD}$, and our cell-based experiments demonstrated that the linker deletion and swap mutations reduce Norrin signaling activity. Further supported by computational modeling and a conformational change observed through HDX-MS, the linker appears to play an important role in transmitting the extracellular ligand-binding signal to the TMD. Together with the linker region, the ICL3 showed a conformational change by Norrin-induced activation of Fzd4. It is widely accepted that agonist-induced activation of class A GPCR leads to conformational change at ICL3 and the cytoplasmic regions of TM5 and TM6 (18–20), although we doubt that Fzd4 in the Wnt signaling pathway shows a similar conformational change as class A GPCR. Cell-based assays and BRET assays suggest that L430 and L433 in ICL3, together with the KTXXXW motif, are important for the interaction with Dvl at the basal level and during activation by Norrin. The molecular details of how the conformational change at ICL3 identified by HDX relates to Dvl binding and downstream signaling remain an open question.

It is unclear whether our findings, such as Norrin-induced conformation changes and the contribution of the linker domain to high-affinity ligand binding, are generally applicable to Fzd–ligand interactions and activation. Unfortunately, in our assay system, we could not detect the response of the Fzd4 mutations to Wnt stimulation because Wnt1 and Wnt3a treatments gave a strong positive signal even without Fzd transfection, possibly because of endogenous Fzd. Norrin and Wnt use different binding modes for Fzd with different coreceptors, such as Tspan12 (28, 29), involved in signaling. It is possible that Fzd4 shows Norrin-induced conformational changes distinct from those of Wnt, despite the fact that both share the canonical signaling pathway. Further structural and functional studies of Fzd are required to examine this possibility.

Methods

Mus musculus Fzd4, $Fzd4_{CRD}$, $Fzd4_{CRDlinker}$, and human Norrin were expressed in *Spodoptera frugiperda* (Sf9) cells. Fzd4 was purified from the membrane fraction, and $Fzd4_{CRD}$, $Fzd4_{CRDlinker}$, and human Norrin were purified from the cell medium by using an affinity column followed by Superdex 200 gel filtration chromatography. Details on the construct information, protein purification, molecular weight determination with a MALS detector, binding experiments using fluorescence size-exclusion chromatography (FSEC) and MST, TOPFlash, immunofluorescence, BRET assays, TBM, and HDX experiments are provided in *SI Appendix, Materials and Methods*.

ACKNOWLEDGMENTS. We thank Dr. William I. Weis (Stanford University) for helpful discussions and Dr. Young-Pil Kim (Hanyang University) for providing the BRET plasmids. This work was supported by the Creative-Pioneering Researchers Program through Seoul National University (H.-J.C.), NSF Grant MCB-1727508 (to W.I.), and National Research Foundation of Korea Grants NRF-2016R1A2A1A05005485 and NRF-2016M3C4A7952630 (to C.S.), NRF-2017K1A3A1A12072316 (to K.Y.C.), and NRF-2016R1A2B4013488 (to H.-J.C.) funded by the Korean government.

1. Logan CY, Nusse R (2004) The Wnt signaling pathway in development and disease. *Annu Rev Cell Dev Biol* 20:781–810.
2. Dann CE, et al. (2001) Insights into Wnt binding and signalling from the structures of two Frizzled cysteine-rich domains. *Nature* 412:86–90.
3. Ye X, et al. (2009) Norrin, Frizzled-4, and Lrp5 signaling in endothelial cells controls a genetic program for retinal vascularization. *Cell* 139:285–298.
4. Berger W (1998) Molecular dissection of Norrie disease. *Acta Anat (Basel)* 162:95–100.
5. Xu Q, et al. (2004) Vascular development in the retina and inner ear: Control by Norrin and Frizzled-4, a high-affinity ligand-receptor pair. *Cell* 116:883–895.
6. Wong H-C, et al. (2003) Direct binding of the PDZ domain of Dishevelled to a conserved internal sequence in the C-terminal region of Frizzled. *Mol Cell* 12:1251–1260.
7. Tauriello DVF, et al. (2012) Wnt/β-catenin signaling requires interaction of the Dishevelled DEP domain and C terminus with a discontinuous motif in Frizzled. *Proc Natl Acad Sci USA* 109:E812–E820.
8. Ke J, et al. (2013) Structure and function of Norrin in assembly and activation of a Frizzled 4-Lrp5/6 complex. *Genes Dev* 27:2305–2319.
9. Chang TH, et al. (2015) Structure and functional properties of Norrin mimic Wnt for signalling with Frizzled4, Lrp5/6, and proteoglycan. *eLife* 4:06554.
10. Janda CY, Waghray D, Levin AM, Thomas C, Garcia KC (2012) Structural basis of Wnt recognition by Frizzled. *Science* 337:59–64.
11. West GM, et al. (2011) Ligand-dependent perturbation of the conformational ensemble for the GPCR beta2 adrenergic receptor revealed by HDX. *Structure* 19:1424–1432.
12. DeBruine ZJ, et al. (2017) Wnt5a promotes Frizzled-4 signalosome assembly by stabilizing cysteine-rich domain dimerization. *Genes Dev* 31:916–926.
13. Nile AH, Mukund S, Stanger K, Wang W, Hannoush RN (2017) Unsaturated fatty acyl recognition by Frizzled receptors mediates dimerization upon Wnt ligand binding. *Proc Natl Acad Sci USA* 114:4147–4152.
14. Petersen J, et al. (2017) Agonist-induced dimer dissociation as a macromolecular step in G protein-coupled receptor signaling. *Nat Commun* 8:226.
15. Wang C, et al. (2013) Structure of the human smoothened receptor bound to an antitumour agent. *Nature* 497:338–343.
16. Byrne EFX, et al. (2016) Structural basis of smoothened regulation by its extracellular domains. *Nature* 535:517–522.
17. Zhang X, et al. (2017) Crystal structure of a multi-domain human smoothened receptor in complex with a super stabilizing ligand. *Nat Commun* 8:15383.
18. Rasmussen SGF, et al. (2011) Crystal structure of the β2 adrenergic receptor-Gs protein complex. *Nature* 477:549–555.
19. Manglik A, Kruse AC (2017) Structural basis for G protein-coupled receptor activation. *Biochemistry* 56:5628–5634.
20. Bang I, Choi HJ (2015) Structural features of β2 adrenergic receptor: Crystal structures and beyond. *Mol Cells* 38:105–111.
21. Weis DD, Wales TE, Engen JR, Hotchko M, Ten Eyck LF (2006) Identification and characterization of EX1 kinetics in H/D exchange mass spectrometry by peak width analysis. *J Am Soc Mass Spectrom* 17:1498–1509.
22. Gayen S, Li Q, Kim YM, Kang C (2013) Structure of the C-terminal region of the Frizzled receptor 1 in detergent micelles. *Molecules* 18:8579–8590.
23. Bertalovitz AC, Pau MS, Gao S, Malbon CC, Wang HY (2016) Frizzled-4 C-terminus distal to KTXXXW motif is essential for normal Dishevelled recruitment and Norrin-stimulated activation of Lef/Tcf-dependent transcriptional activation. *J Mol Signal* 11:1.
24. Milhem RM, Ben-Salem S, Al-Gazali L, Ali BR (2014) Identification of the cellular mechanisms that modulate trafficking of frizzled family receptor 4 (FZD4) missense mutants associated with familial exudative vitreoretinopathy. *Invest Ophthalmol Vis Sci* 55:3423–3431.
25. Gammons MV, Renko M, Johnson CM, Rutherford TJ, Bienz M (2016) Wnt signalosome assembly by DEP domain swapping of Dishevelled. *Mol Cell* 64:92–104.
26. Strakova K, et al. (2017) The tyrosine $Y250^{2.39}$ in Frizzled 4 defines a conserved motif important for structural integrity of the receptor and recruitment of Disheveled. *Cell Signal* 38:85–96.
27. Zhang C, et al. (2017) Norrin-induced Frizzled4 endocytosis and endo-lysosomal trafficking control retinal angiogenesis and barrier function. *Nat Commun* 8:16050.
28. Junge HJ, et al. (2009) TSPAN12 regulates retinal vascular development by promoting Norrin- but not Wnt-induced FZD4/beta-catenin signaling. *Cell* 139:299–311.
29. Lai MB, et al. (2017) TSPAN12 is a Norrin co-receptor that amplifies Frizzled4 ligand selectivity and signaling. *Cell Rep* 19:2809–2822.